PHYSICAL REVIEW B **84**, 205410 (2011)

Universal scaling relations for the thermoelectric power factor of semiconducting nanostructures

Jane E. Cornett[1] and Oded Rabin[1,2,*]
[1]*Department of Materials Science and Engineering, University of Maryland, College Park, Maryland 20742, USA*
[2]*Institute for Research in Electronics and Applied Physics, University of Maryland, College Park, Maryland 20742, USA*

(Received 2 June 2011; revised manuscript received 18 August 2011; published 11 November 2011)

We present a parametric analysis of the thermoelectric power factor of single-carrier semiconductors for nanowires, thin films, and bulk. We consistently find a reduction in the peak power factor in many-subband nanostructures compared to bulk, independent of the specific materials parameters, system geometry, or dimensionality. A universal relation between the optimal power factor and the system size, common to all single-carrier materials, is developed for nanowires and thin films. The common nonmonotonic trend highlights the competing effects of quantization and degeneracy on the transport properties of semiconductor nanostructures. The model predicts decreases of up to 28% and 22% in the peak power factor in nanowires and thin films, respectively, relative to the bulk value. This study provides insights to successful figure-of-merit enhancement strategies.

DOI: 10.1103/PhysRevB.84.205410 PACS number(s): 73.50.Lw, 72.20.Fr, 72.20.Pa, 73.63.Nm

I. INTRODUCTION

Thermoelectric materials are characterized by their dimensionless figure of merit $ZT = \sigma S^2 T/\kappa$, which depends on the electrical conductivity σ, Seebeck coefficient S, total thermal conductivity κ, and the absolute temperature T.[1] A large portion of recent work in the field has focused on synthesis and characterization of nanostructures for thermoelectric applications due to two predicted benefits over bulk: (1) an increase in the thermoelectric power factor ($PF = \sigma S^2$) due to distortion of the electronic density-of-states (DOS) function and (2) a decrease in the lattice thermal conductivity κ_l as a result of increased phonon boundary scattering. While improvements in ZT have been demonstrated when moving from bulk to nanoscale, in most cases this is entirely due to a substantial decrease in the lattice thermal conductivity, and no improvement is seen in the electronic transport properties.[2–6]

The original models for thermoelectric transport in nanostructures, developed in 1993 by Hicks and Dresselhaus, predicted monotonic increases in PF and ZT with decreasing system size both in nanowires and in thin films.[7,8] The models assume that the conduction band consists of a single subband, finding that PF has an r^{-2} dependence on nanowire radius (r) and an a^{-1} dependence on film thickness (a). However, the single-subband assumption, referred to as the electric quantum limit,[9] is valid only for very small structures in which the quantum confinement energies are significantly larger than $k_B T$. For larger structures, additional subbands have energies close to the Fermi energy and their contribution to transport cannot be neglected. We recently developed a many-subband model, which takes into account the additive effect of these additional subbands, and have shown that in cylindrical InSb nanowires with $r > 17$ nm, *PF increases* monotonically with nanowire radius in sharp contrast to the predictions of the previous models.[10] The increase in PF was found to originate from an increase in the electronic DOS as the number of contributing subbands increases with r. This trend could not have been identified by calculations based on the single-subband model.

Given the significant impact the new model may have on future directions of thermoelectric research, a full analysis of the many-subband model was carried out in order to identify the set of circumstances that lead to a clear deviation from the behavior identified by Hicks and Dresselhaus. Here, we report room temperature PF calculations as a function of system size for nanowires with both circular and square cross-sections and for thin films. Focusing on single-carrier semiconductors, the effect of varying band parameters on the relation between power factor and system size is investigated. We provide evidence that the trends observed in InSb nanowires are material independent and that size reduction alone rarely leads to an enhancement in the thermoelectric power factor. The analysis shows that for all systems studied, regardless of geometry, dimension, or band parameters, PF has a nonmonotonic dependence on system size and its values are below the bulk value for most of the size range studied. Universal relations between PF and system size, which apply to any single-carrier material of this type, are then derived.

This paper is organized as follows: Sec. II gives a detailed explanation of the approach taken to calculate the complete subband structure of the nanowires and thin films and the transport equations solved for each system. The dependence of PF on band parameters and system size, as well as universal PF curves, is presented in Sec. III. Section IV addresses several model assumptions. Section V provides an outlook for future research in the field of nanoscale thermoelectrics based on the findings described here.

II. THEORY

The thermoelectric transport properties of a single-carrier semiconductor are obtained by solving the Boltzmann transport equation in the presence of an electric field and a temperature gradient. For a given temperature T, the electrical conductivity and Seebeck coefficient can be expressed via[11]

$$\sigma = \mathbf{L}^{(0)}$$
$$S = -\mathbf{L}^{(1)}/(eT \cdot \mathbf{L}^{(0)}), \tag{1}$$

where e is the charge of an electron and

$$\mathbf{L}^{(\alpha)} = e^2 \int \frac{d\mathbf{k}}{4\pi^3}\left(-\frac{\partial f}{\partial E}\right)\tau(E(k))v(\mathbf{k})v(\mathbf{k})(E(\mathbf{k}) - E_f)^{\alpha}. \tag{2}$$

In Eq. (2), $\mathbf{k}$ is the electron wavevector, f is the energy-dependent Fermi-Dirac distribution, $\tau(E(k))$ is the electron relaxation time, $v(\mathbf{k})$ is the electron group velocity, E_f is the Fermi energy, and $E(\mathbf{k})$ is the energy dispersion relation for electrons. For all systems studied here, Eqs. (1) and (2) were solved for an electron relaxation time constant with respect to both energy and system size. The band gap of the material is assumed large enough that a single majority carrier is present—taken to be electrons in the conduction band without loss of generality. We take the transport direction, indicated as the x-direction in all systems studied, to be along the nanowire or in the plane of the thin film. The general case of an ellipsoid-of-revolution Fermi surface is developed in the following discussion, while in Sec. III A. calculation results are introduced for the case of a spherical Fermi surface. The effective mass in the x-direction, the direction of transport, is denoted $m_{||}^*$, while the effective masses in the y- and z-directions, which are taken to be equal, are denoted $m_{\perp}^*$. To study the effect of the band parameters on the relation between PF and system size, calculations were done for effective mass values of $0.01m_0$–$0.06m_0$ (where $m_0 = 9.1 \times 10^{-31}$ kg), carrier mobility values of $\mu = 1 \times 10^5 - 7 \times 10^5 \text{cm}^2/\text{V-s}$, and relaxation times of $\tau = 5 \times 10^{-13} - 2 \times 10^{-12}$s. These values are typical of single-crystal thermoelectric materials.

A. Transport equations in one dimension

1. *Circular cross-section*

Based on the effective mass theorem, the electron wave function $\mathbf{\Psi}(\mathbf{r})$ can be found by solving the following Schrodinger equation[11]:

$$-\frac{\hbar^2}{2}\nabla \cdot \boldsymbol{\alpha} \cdot \nabla\mathbf{\Psi}(\mathbf{r}) + V(\mathbf{r})\mathbf{\Psi}(\mathbf{r}) = E\mathbf{\Psi}(\mathbf{r}), \tag{3}$$

where $\boldsymbol{\alpha}$ is the inverse effective mass tensor, $V(\mathbf{r})$ is the confining potential created by the nanowire boundary, and E is the electron eigenenergy. For cylindrical nanowires, the imposed boundary conditions are that $\mathbf{\Psi}(\mathbf{r})$ vanishes at the nanowire boundary and that it remains finite elsewhere. Due to the rotational symmetry of the single Fermi pocket considered here, Eq. (3) was solved analytically. However, numerical models have been developed and can be utilized for more complex band structures.[12–14]

Studying transport along the axis of the nanowire, taken to be in the x-direction, the eigenenergies of Eq. (3) are of the form

$$E(\mathbf{k}) = E_{\text{nm}}(k_x) = \frac{\hbar^2 k_x^2}{2m_{||}^*} + E_{\text{nm}}, \tag{4}$$

where E_{nm} is the quantized energy level resulting from confinement in the y- and z-directions. The energy level E_{nm}, referred to as the "subband energy," marks the bottom edge of the subband dispersion relation. For a cylindrical nanowire of radius r, these subband energies are given by $E_{\text{nm}} = j_{\text{nm}}^2\hbar^2/2m_{\perp}^* r^2$, where j_{nm} is the nth root of the mth-order Bessel function of the first kind. The lowest 300 subband energies were calculated for each r.

Thermoelectric transport properties for cylindrical nanowires were calculated by solving the following one-dimensional (1D) form of Eq. (2):

$$\mathbf{L}^{(\alpha)} = \sum_{\text{nm}} 2\frac{e\mu\sqrt{2m_{||}^*}}{\pi^2 r^2 \hbar}\int_{E_{\text{nm}}}^{\infty} dE\sqrt{E - E_{\text{nm}}} \cdot \left(-\frac{\partial f}{\partial E}\right) \cdot (E - E_f)^{\alpha}, \tag{5}$$

where we have used the relations $\tau = \mu m_{||}^*/e$ and $v(\mathbf{k}) = (1/\hbar)(dE/d\mathbf{k})$. All preceding energies are given relative to the conduction band edge of bulk. The sum over the contributions of all subbands in Eq. (5) was truncated after 300 subbands—a sufficient number to reach convergence of PF values. Transport property calculations were performed using Eqs. (1) and (5) for nanowire radii between 1 and 100 nm. For each r, PF was optimized with respect to the Fermi energy, and its maximum value was used in the following analysis.

The distinction between the many-subband model presented here and the single-subband model developed by Hicks and Dresselhaus is the summation in Eq. (5). Without this summation, only the contribution of the lowest subband is calculated. This single subband energy E_{11} increases as r decreases; however, except for a global energy shift, the DOS function remains unchanged [Fig. 1(a)]. Without the summation, the value of the integral in Eq. (5) is independent of r, depending only on the energy difference $E_f - E_{11}$. As a consequence, in the single-subband model, the Fermi energy that maximizes PF is "pinned" to the subband energy, regardless of the nanowire radius [Fig. 1(b)]. The optimal Fermi energy therefore needs to be determined only once, for an arbitrary value of r. The r^{-2} dependence of PF in the Hicks and Dresselhaus model emerges from the energy-independent form factor in $\mathbf{L}^{(\alpha)}$ and in σ. Physically, the r^{-2} dependence corresponds to the cross-sectional scaling of the conductivity of a quantum wire as the radius is varied, maintaining a single operative conduction channel.

2. *Square cross-section*

For nanowires with a square cross-section, the eigenenergies of Eq. (3) were solved for with the boundary condition that the electron wave function vanishes at the surface of the nanowire. The resulting quantized energy levels corresponding to quantum numbers n and m are of the form $E_{nm} = \hbar^2\pi^2(n^2 + m^2)/2m_{\perp}^* l^2$, where l is the wire width. As with the cylindrical nanowires, the lowest 300 subbands were considered for each l. For this square geometry, Eq. (2) becomes

$$\mathbf{L}^{(\alpha)} = \sum_{\text{nm}} 2\frac{e\mu\sqrt{2m_{||}^*}}{\pi l^2 \hbar}\int_{E_{nm}}^{\infty} dE\sqrt{E - E_{\text{nm}}} \cdot \left(-\frac{\partial f}{\partial E}\right) \cdot (E - E_f)^{\alpha}. \tag{6}$$

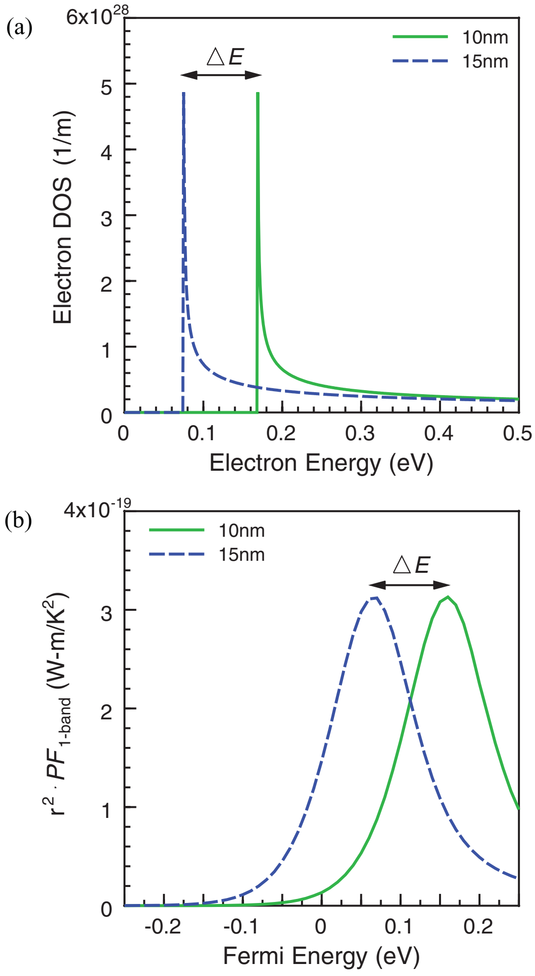

FIG. 1. (Color online) (a) The 1D electronic DOS functions, assuming the single-subband model, for cylindrical nanowires of radii 10 and 15 nm. (b) The single-subband PF, normalized by multiplying by r^2, as a function of Fermi energy for these same two nanowires. The energy ΔE is the same in both plots, indicating that in the single-subband model, the Fermi energy that optimizes PF is pinned to the subband energy.

Transport properties were calculated as a function of Fermi energy for wire widths between 2 and 200 nm. PF values were optimized with respect to the Fermi energy for each l.

Transport Eqs. (5) and (6) appear identical for cylindrical and square nanowires of the same cross-sectional area; however, the sets of subband energies E_{nm} are different for the two geometries. The number of subbands used was sufficient to achieve convergence in the sums of Eqs. (5) and (6), as long as $m_\perp^* r^2$ did not exceed $130 m_0$ nm^2 and $m_\perp^* l^2$ did not exceed $469 m_0$ nm^2.

B. Transport equations in two dimensions

For two-dimensional (2D) thin films, we took the z-axis to be perpendicular to the film and the electric field and temperature gradient in the x-direction. For this system, the imposed boundary condition is a vanishing wave function $\mathbf{\Psi}(\mathbf{r})$ at the thin film surfaces. The eigenenergy solutions of Eq. (3) are then given by

$$E(\mathbf{k}) = E_n(k_x,k_y) = \frac{\hbar^2}{2}\left(\frac{k_x^2}{m_{||}^*} + \frac{k_y^2}{m_\perp^*}\right) + E_n, \tag{7}$$

where E_n is the "subband energy," the quantized energy level resulting from confinement, marking the bottom edge of the subband dispersion relation. The nth subband energy is given by the equation $E_n = \hbar^2\pi^2 n^2/2m_\perp^* a^2$, where a is the film thickness. Subband energies were calculated for $n = 1$–300.

The thermoelectric transport properties were calculated for thin films as a function of Fermi energy for film thicknesses between 2 nm and 1 μm by solving the 2D form of Eq. (2):

$$\mathbf{L}^{(\alpha)} = \sum_n \frac{e\mu m_{||}^*}{\pi\hbar^2 a}\int_{E_n}^{\infty} dE\,(E-E_n)\cdot\left(-\frac{\partial f}{\partial E}\right)\cdot(E-E_f)^{\alpha}, \tag{8}$$

where the sum is taken over all subbands. PF values were then optimized with respect to the Fermi energy for each a. Summing over 300 subbands, Eq. (8) converged as long as $m_\perp^* a^2$ did not exceed $13\,000 m_0$ nm^2.

C. Transport equations in three dimensions

Transport property calculations were also carried out for three-dimensional (3D) systems to determine the effect of changing the single-band parameters on transport behavior. In three dimensions, Eq. (2) can be written as[8]

$$\mathbf{L}^{(\alpha)} = \frac{e\mu(2m_{||}^*)^{3/2}}{3\pi^2\hbar^3}\int_0^{\infty} dE\,(E)^{3/2}\cdot\left(-\frac{\partial f}{\partial E}\right)\cdot(E-E_f)^{\alpha}, \tag{9}$$

where the parabolic dispersion relation is now given by $E(\mathbf{k}) = \frac{\hbar^2}{2}(\frac{k_x^2}{m_{||}^*} + \frac{k_y^2+k_z^2}{m_\perp^*})$. For each set of materials parameters, PF was optimized with respect to the Fermi energy.

III. RESULTS AND DISCUSSION

A. Transport properties

1. Effect of band parameters

The thermoelectric power factor, calculated as a function of radius r for cylindrical nanowires assuming an isotropic effective mass m^* ($m_{||}^*/m_\perp^* = 1$), is shown in Fig. 2. The solid (blue) lines in Fig. 2(a) and 2(b) were calculated assuming the effective mass and mobility values of InSb. As we have previously reported,[10] this curve exhibits different behavior in two distinct size ranges: (1) for radii $\leqslant$ 19 nm, confinement of the electrons is strong and PF increases with decreasing r, and (2) for radii $>$ 19 nm, confinement is weak and the subbands become close in energy (nearly degenerate), resulting in an increase in PF with increasing r. Figure 2 also includes PF versus r curves for other values of the band parameters. Figure 2(a) shows the effect of changing the effective mass while maintaining a constant mobility. Two overall trends can be seen as the effective mass is varied. First, PF increases with increasing effective mass for each r. Second, the minimum in PF (which is seen in each of the

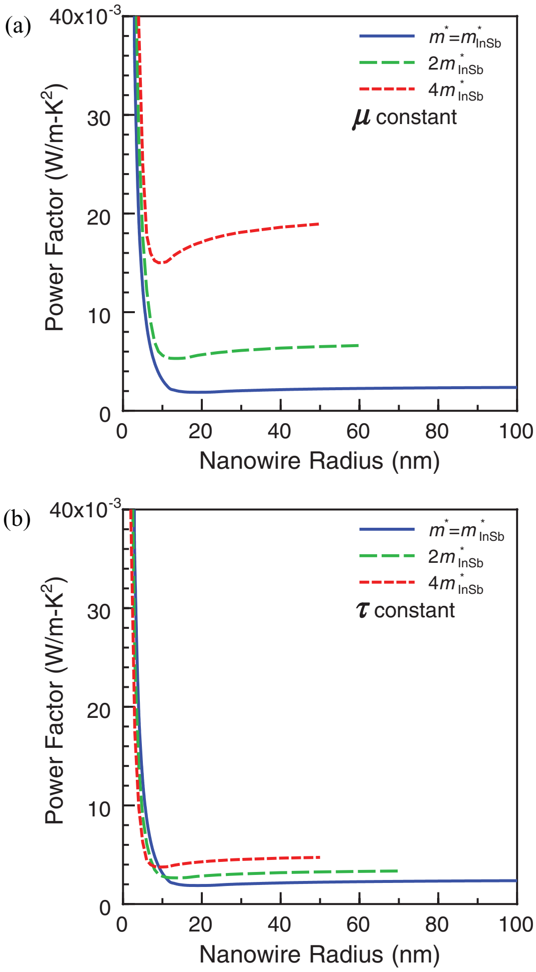

FIG. 2. (Color online) Power factor as a function of radius for cylindrical nanowires. The effective mass is varied between $0.013m_0$ and $0.052m_0$ while (a) the mobility value is fixed to 70 000 cm^2/V-s or (b) the relaxation time is fixed to 5×10^{-13} s.

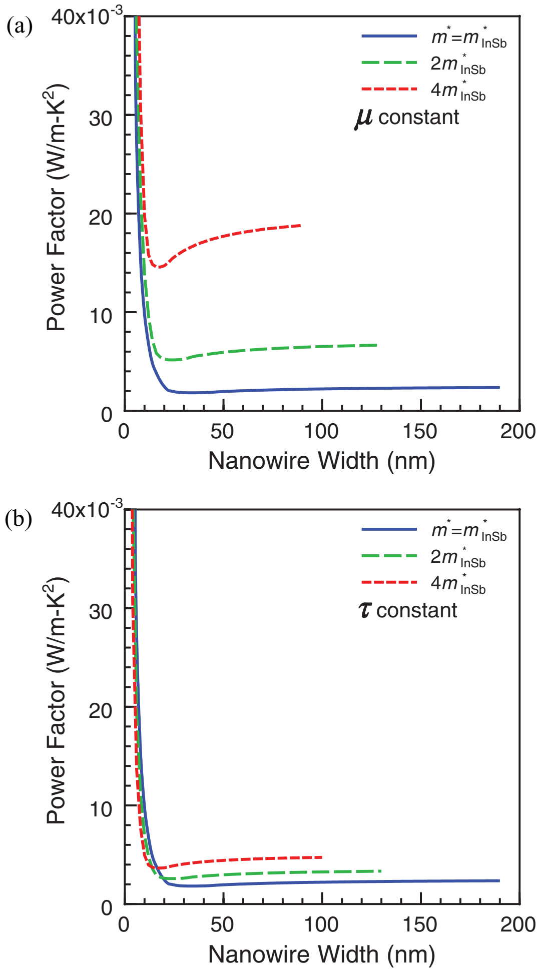

FIG. 3. (Color online) Power factor as a function of wire width for square nanowires. The effective mass is varied between $0.013m_0$ and $0.052m_0$ while (a) the mobility value is fixed to 70 000 cm^2/V-s or (b) the relaxation time is fixed to 5×10^{-13} s.

three curves) becomes narrower and shifts to lower nanowire radii as the effective mass increases, indicative of decreasing confinement. Figure 2(b) shows the effect of changing the effective mass while maintaining a constant relaxation time. Despite this difference, the minima in the PF curves again become narrower and fall lower in r as the effective mass is increased, similar to the trend seen in Fig. 2(a). Furthermore, when comparing systems with the same effective mass (e.g., the short-dashed red curves in Fig. 2(a) and 2(b)), we find that PF increases linearly with electron mobility. The plots in Fig. 2 indicate that the minimum in PF, corresponding to the divide between regions of strong confinement (small r) and regions of weak confinement (large r), is a feature universal to all circular nanowires in single-carrier systems regardless of the particular materials parameters (carrier effective mass and mobility).

2. *Effect of system shape and dimensionality*

Transport property calculations were also done for nanowires with a square cross-section as a function of the wire width l. The optimal PF values for square nanowires with various values of the electron effective mass but the same mobility are compared as a function of l in Fig. 3(a). Figure 3(b) compares PF calculated for various effective mass values, keeping the electron relaxation time constant. A minimum is seen for each system investigated, regardless of the specific materials parameters. As the effective mass is increased, the minimum becomes narrower and occurs for smaller nanowires. These results indicate that these trends in the thermoelectric transport phenomenon are not unique to either a specific material or a specific nanowire geometry.

Analogous transport property calculations were done for 2D thin films as a function of film thickness a. The optimized PF is shown as a function of a for model systems with various electron effective mass values and the same mobility in Fig. 4(a) and for systems with various effective masses and the same relaxation time in Fig. 4(b). The nonmonotonic relation between PF and a persists in all systems studied. For InSb, the minimum PF value is seen for a film thickness of 27 nm, confirming that smaller system sizes are required for strong confinement in 2D films as compared with 1D nanowires (for which the minimum is located at $2r = 38$ nm or $l = 34$ nm).

For the nanostructures discussed here, we identified several common trends in the relation between optimal PF and

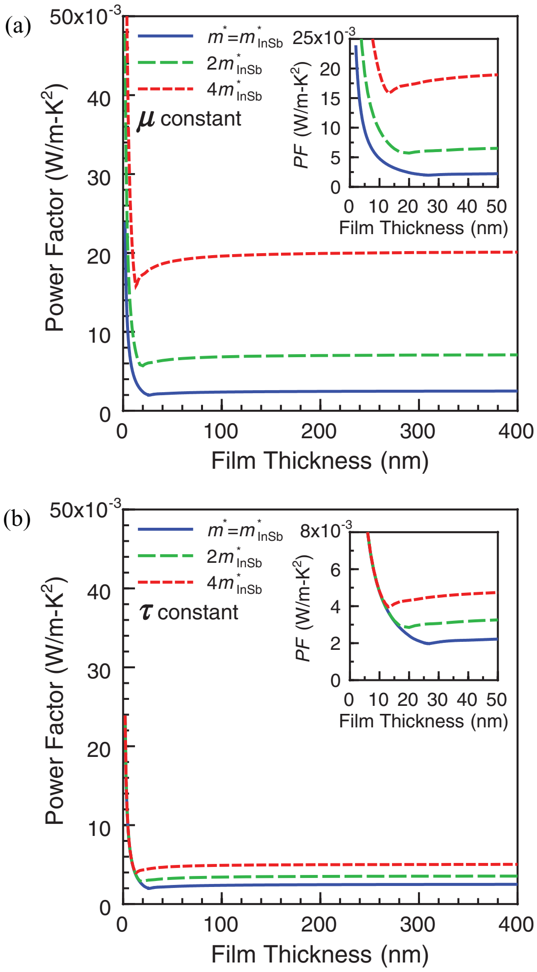

FIG. 4. (Color online) Power factor as a function of thickness for thin films. The effective mass is varied between $0.013m_0$ and $0.052m_0$ while (a) the mobility value is fixed to 70 000 cm^2/V-s or (b) the relaxation time is fixed to 5×10^{-13} s. The insets show magnified portions of the corresponding plots, which include the minima in PF for each curve.

system size and how this relation is affected by changes to the single-carrier parameters: (1) For all structures (cylindrical nanowires, square nanowires, and thin films), increasing the electron effective mass results in a narrower minimum, shifted to a smaller system size. (2) For all structures and system sizes, PF increases monotonically with electron mobility. (3) For all materials and systems investigated, the dependence of PF on system size can be split into two size ranges based on the dominant physical behavior. For smaller systems, confinement is strong and PF increases with decreasing size. For larger systems, confinement is weaker and PF increases with increasing size. A minimum in PF, which falls 22%–28% below the bulk value, separates these two regions. As shown later, this behavior is the result of the fundamental changes in the DOS function within the scope of the constant relaxation time approximation (CRTA).

The trends in the thermoelectric transport in all nanostructures of isotropic single-carrier materials are similar and can be explained by a generalized theoretical framework that considers the influence of size on the DOS function and on the number of subbands that contribute to transport. For structures in which a single subband contributes to transport, the subband essentially acts as a lone conduction channel for electrons with a size-independent conductance. A decrease in the system size therefore translates to an increase in the effective conductivity of the system. For PF of cylindrical nanowires, this corresponds to an r^{-2} dependence on radius. For thin films, PF follows an a^{-1} dependence on film thickness. As the size of the nanostructure increases, the subbands become closer together in energy. There is a critical size at which additional subbands become relevant, marked by the minimum in the PF curves. In the many-subband size range, an increase in the number of subbands leads to an increase in PF—*despite* the corresponding increase in system size. Thus, when many subbands contribute to transport, degeneracy as opposed to confinement becomes the dominating effect.

While the qualitative behavior of all preceding systems is similar, the exact sizes corresponding to the PF minimum, as well as the size required for improvement in PF over bulk, depend on the specific materials parameters used. In the absence of a complete understanding of the relations among thermoelectric power factor, system size, and materials parameters, in-depth modeling of each material is required to extract this practical information.

We proceed to introduce a universal model for PF as a function of size. Given a single-carrier material with an ellipsoid-of-revolution Fermi pocket, this universal model provides the full description of the size dependence of the optimal PF of the system, requiring no further computational effort.

B. Universal scaling relations

The universal scaling relations are derived for each nanostructure (cylindrical nanowires, square nanowires, and 2D thin films) from the mass, mobility, and size dependences of PF. For each structure, the expression for PF consists of a product of two terms [see Eqs. (1), (5), (6), and (8)]: an energy independent coefficient, and a quotient of integrals that depends on the quantized energy levels and the Fermi energy. While the preceding discussion focused on systems with a spherical Fermi pocket, the universal scaling relations presented here apply to systems in which the effective mass perpendicular to the transport direction ($m_\perp^*$) is not necessarily equal to that parallel to the transport direction ($m_{||}^*$).

1. Cylindrical nanowires

For cylindrical nanowires of cross-sectional area πr^2, the energy-independent coefficient is proportional to the product $\frac{\mu\sqrt{m_{||}^*}}{\pi r^2}$ [in contrast, the bulk PF follows $\mu(m_{||}^*)^{3/2}$]. The subband energies are proportional to $\frac{1}{m_\perp^*\pi r^2}$, meaning that systems with equal $m_\perp^* r^2$ will have identical energy levels and thus the energy-dependent integral portion of PF will be identical. Normalizing the nanowire PF with respect to the bulk value and plotting this normalized PF as a function of $(\frac{m_\perp^*}{m_0})r^2$ (as opposed to r) gives rise to the curve shown in Fig. 5. This transformation causes all of the PF data calculated and shown in Fig. 2 to merge into a single curve. This curve is common to all cylindrical nanowires of single-carrier

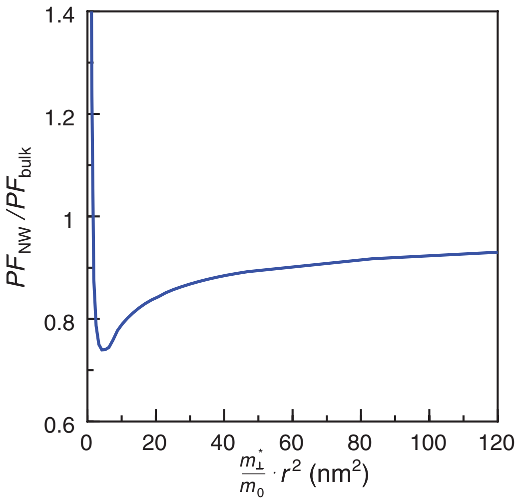

FIG. 5. (Color online) The universal curve for cylindrical nanowires (NWs).

materials with a spherical Fermi surface, as well as those with an ellipsoid-of-revolution Fermi surface. The universal curve exhibits a minimum (26% below the bulk value) for $(\frac{m_\perp^*}{m_0})r^2 = 4.7$ nm^2. The normalized PF values approach 1 in the limit of large $(\frac{m_\perp^*}{m_0})r^2$, and $(\frac{m_\perp^*}{m_0})r^2 \leqslant 1.6$ nm^2 is required for an improvement in PF over bulk.

2. *Square nanowires*

The energy-independent coefficient of PF is proportional to $\frac{\mu\sqrt{m_\parallel^*}}{l^2}$ for square nanowires of cross-sectional area l^2, and the subband energy levels are proportional to $\frac{1}{m_\perp^* l^2}$. The universal curve for square nanowires is found by appropriate scaling of the data: PF values are normalized with respect to the bulk value and are plotted as a function of $(\frac{m_\perp^*}{m_0})l^2$ as opposed to l (Fig. 6). This transformation causes all PF data calculated and shown in Fig. 3 to merge into a single curve. The minimum of this universal curve is located at $(\frac{m_\perp^*}{m_0})l^2 = 15.0$ nm^2, with a PF value 28% below the bulk value. To see an increase in PF over the bulk value, systems must satisfy $(\frac{m_\perp^*}{m_0})l^2 \leqslant 5.1$ nm^2.

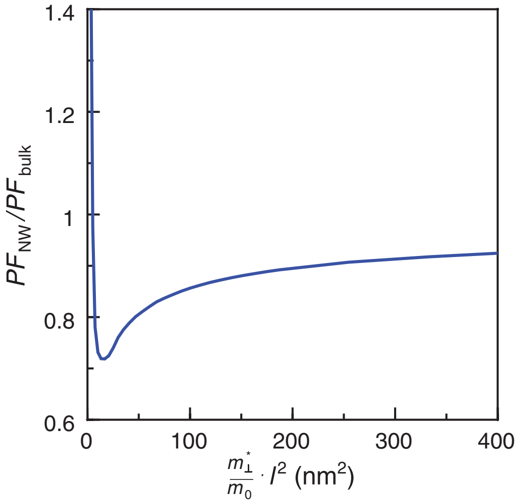

FIG. 6. (Color online) The universal curve for square nanowires.

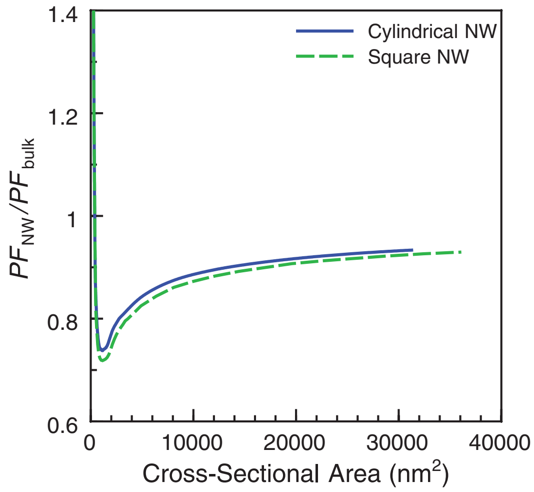

FIG. 7. (Color online) Normalized power factor as a function of the cross-sectional area for cylindrical and square nanowires (NWs).

Figure 7 compares PF, normalized relative to the bulk value, as a function of the nanowire cross-sectional area for cylindrical and square geometries. The electron effective mass value of InSb is assumed. The overall trends are similar, exhibiting minima near cross-sectional areas of ~1100 nm^2. For areas $<$ 1100 nm^2, a single subband contributes to transport and PF values for the two geometries are identical. For larger systems in which additional subbands contribute, PF values of cylindrical nanowires differ from those of square nanowires because the subband energy separations for the two geometries are different.

3. *Thin films*

In 2D systems, the energy-independent coefficient of PF depends on carrier mass, mobility, and film thickness via the

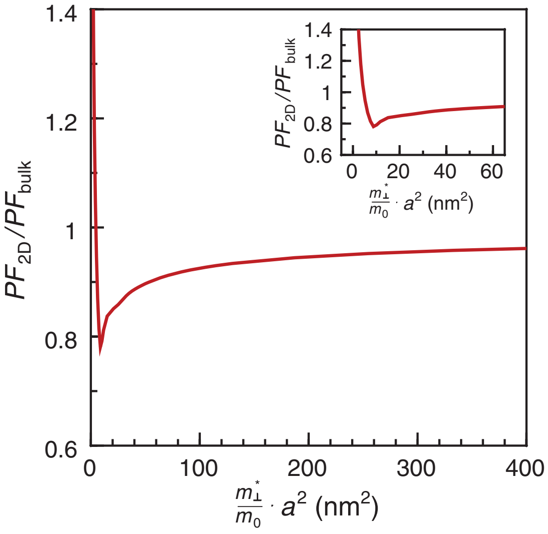

FIG. 8. (Color online) The universal curve for thin films. The inset shows a magnified portion of the plot, including the PF minimum.

factor $\frac{\mu m^*_\parallel}{a}$. The subband energies are proportional to $\frac{1}{m^*_\perp a^2}$. Scaling PF values relative to the bulk value and plotting them as a function of $(\frac{m^*_\perp}{m_0})a^2$ gives rise to the universal curve in Fig. 8. With the preceding transformation, all data shown in Fig. 4 merge into a single curve. The minimum here occurs at $(\frac{m^*_\perp}{m_0})a^2 = 9.1$ nm^2 (falling just 22% below the bulk value), while improvement in PF over bulk requires $(\frac{m^*_\perp}{m_0})a^2 \leqslant$ 4.7 nm^2. These values are small relative to those found in nanowires due to the reduced degree of confinement in 2D systems.

IV. ADDITIONAL MODEL CONSIDERATIONS

The Hicks and Dresselhaus models helped jump-start the field of nanothermoelectrics. These models are still relevant almost two decades later but are often wrongly applied to materials systems beyond their intended scope without significant scrutiny. To avoid future misinterpretations of our model, this section discusses in detail its scope and limitations.

The model developed here, leading to the nonmonotonic dependence of PF on system size, is applicable to any semiconductor whose carriers can be characterized by a single effective mass tensor and a single mobility tensor. These tensors are assumed to be size independent, indicating that the dominant scattering mechanism and the locations of the carrier pockets in the Brillouin zone should be the same for the bulk and the low-dimensional structures. This model can be applied to materials with degenerate valleys. Utilization of the universal curves in Figs. 5, 6, and 8 should be restricted to dispersion relations that lead to ellipsoid-of-revolution Fermi surfaces. All calculations were done at room temperature ($T =$ 300 K). Deviations due to extreme low and high temperatures have not been fully investigated at this point.

The model uses the CRTA. An average τ (deduced from transport data) is assigned to all electron states independent of electron energy and system size. When considering the scattering mechanisms in various materials systems and heterogeneous device structures, a complex pattern of size dependence emerges. Varying the system size affects the mobility through (1) the change in the dispersion relation of the electronic subbands; (2) the change in the optimal E_f, and therefore in the carrier concentration, which maximizes the thermoelectric properties; (3) phonon confinement and resulting changes in the phonon dispersion relation; and (4) interface effects, including surface roughness, charge accumulation at interfaces and buried in adjacent materials, and boundary conditions imposed on the electrons and the phonons in the system. Examples of calculations of PF for narrow-width semiconductor nanowires (including InSb) considering the material-specific scattering in detail can be found in Refs. 15–17. Typically, the scattering rates gradually approach their bulk values as the system size increases, and large deviations from the bulk are only observed below a characteristic size associated with the scattering mechanism. The CRTA can be justified as long as the system size is larger than this critical size. Theoretical and experimental work suggests that in many instances the critical size is found to be <20 nm. Considering scattering of electrons by acoustic phonons and polar optical phonons, carrier mobility calculated for GaAs thin films is not affected by film thickness down to ~10 nm.[15,18] Theoretical investigations of low-field carrier mobility in silicon-on-insulator inversion layers[19] and nanowire transistors[20] have included additional scattering mechanisms (surface roughness and coulomb scattering). Carrier mobility limited by these mechanisms was again shown to be strongly size dependent only for systems smaller than ~10 nm; for larger structures, the mobility varies slightly and deviates from the value calculated for an inversion layer in micron-sized transistors by a maximum of 20%. The effect of phonon confinement on carrier mobility has also been investigated in Si nanowires[21] and silicon-on-insulator thin films,[22] and it is predicted to be most significant in systems with critical dimensions on the order of the thermal phonon wavelength (<10 nm for room temperature Si). Experimental work on lightly doped silicon-on-insulator films has verified that the mobility stays within 20% of the bulk value for films as small as 9.4 nm,[23] and studies of the electron conductivity in metallic thin films have similarly shown that very small film thicknesses are required for a significant deviation from the bulk value.[24–26] These examples are remarkable in the sense that they provide qualitatively the same trend in the size dependence for mobilities that vary over orders of magnitude and are dominated by a variety of physical processes. Experimental values of the mobility in nanowire systems are scarcer and often limited by boundary roughness scattering. However, bulklike mobilities have been reported in <20-nm-diameter *p*-type Si nanowires[27] and *n*-type GaN nanowires.[28]

To date, theoretical and experimental work indicates that the electron mobility is approximately size independent, approaching the bulk value, for systems > 20 nm. In this size range, which includes the majority of structures discussed here, a detailed investigation of the various relevant scattering mechanisms is expected to yield at most a 20% variation in the magnitude of PF. The modifications are expected to increase as the system size decreases and the approximation of a constant relaxation time becomes invalid. The most important trend derived using our model—the reduction of PF value in nanostructures vs bulk—is found in the *intermediate* size range and consequently is expected to be consistent with more detailed models considering various material-specific scattering mechanisms. For systems below the critical size of 20 nm, however, the CRTA adopted in this work is not reliable. The trends observed for these highly confined systems should be revisited through the investigation of specific materials and their size-dependent scattering rates. For example, the power factor may never exceed the bulk value due to size-dependent scattering in small nanostructures.[29] Such material-specific considerations were avoided in an effort to maintain the generality of our results and prevent the underlying physics from being lost in the details, but they should be kept in mind. In addition, while the experimental results cited earlier indicate a weak dependence of carrier mobility on sizes >20 nm, they give no indication of the evolution of the energy-dependent $\mu(E)$ as the system size is varied.[22] A better understanding of this relation is crucial for improved accuracy in transport property calculations. These complications notwithstanding, the low-dimensional multiple-subband systems have a DOS profile that is undesirable for a thermoelectric material.

The reduced DOS in nanostructures and its detrimental effect on the thermoelectric PF have not been discussed in the literature, though several mechanisms leading to a comparable decrease in PF in nanowires and thin films have been identified in the past. A related mechanism is the lifting of carrier pocket degeneracy due to quantization—however, this is a material-specific phenomenon that imposes conditions on the band structure of the material and the crystallographic orientation of the nanowire.[30] A decrease in carrier mobility, due to increased polar optical phonon scattering rates in small structures, can also lead to an unfavorable decrease in thermoelectric properties.[15,31] As mentioned earlier, this mechanism is most effective for remarkably small structures (<20 nm), where single-subband conditions apply. Finally, size reduction may result in loss of confinement of the electronic states: in superlattice thin film and nanowire structures with finite confinement potentials, reduction in size can lead to a reduced PF due to increased carrier tunneling when the barriers become very narrow.[15,31] While these examples are relevant to the design of thermoelectric nanostructures, the phenomenon reported here is of greater significance. The nonmonotonic behavior shown here is not material specific and is predicted for *any individual carrier pocket*. The effect is pronounced in weakly confined electronic systems, corresponding to the size range of most experimental nanowire systems that can be reproducibly fabricated today.

Generally, the optimization of PF is a step toward the goal of maximizing ZT. We emphasize that the functions $PF(r)$ and $ZT(r)$ (or $PF(a)$ and $ZT(a)$, etc.) do not necessarily follow the same trends, since the lattice contribution to thermal conductivity often has a strong size dependence. Thus, when size reduction significantly decreases the thermal conductivity, a monotonic increase in ZT with confinement is possible, as has been observed experimentally.

For all nanostructures and bulk systems investigated here, the Fermi energy (i.e., doping level) has been chosen such that PF is maximized for each system size. The Fermi energy of consideration (or optimal doping) is different depending on whether PF or ZT is maximized. The universal curves can be derived only when PF values are optimized. Optimizing ZT requires inclusion of the size dependence of the lattice thermal conductivity of a particular material. Nevertheless, the universal curves shown here can be considered the best-case scenario for PF variation with size: for any given r, the percent reduction in PF values below the bulk value is even greater when the Fermi energy is adjusted to optimize ZT. The adjustment in the Fermi energy is directly related to the ratio of the electron and the lattice contributions to thermal conductivity. When $\kappa_l \gg \kappa_e$, the Fermi energy dependence of ZT is similar to that of PF, and the E_f adjustment is small. As κ_l is largest in bulk structures, the Fermi energy adjustment is smaller in 3D than in 1D or 2D systems. The difference between *optimal PF* and PF evaluated at the Fermi energy that optimizes ZT increases with the magnitude of the E_f adjustment. Consistent with this, we calculated for cylindrical InSb nanowires a 26% decrease in PF relative to bulk when E_f is selected to maximize PF (Fig. 2) and a 38% decrease in PF versus bulk when selecting E_f to maximize ZT.[10] The radius corresponding to the minimum in PF for cylindrical InSb nanowires varies slightly, from 19 nm (when optimizing with respect to PF) to 17 nm (when optimizing with respect to ZT).

V. IMPLICATIONS ON FUTURE RESEARCH

The universal curves developed here present a set of guidelines for future research, both theoretical and experimental. We have shown that improvements in the thermoelectric power factor are difficult to come by in single-carrier materials. Further work should focus on possible ways to utilize nanostructures to compensate for the anticipated decrease in PF. Several approaches for achieving this can be derived from the model:

(1) Engineering the band structure through quantum confinement, such that the carriers shift to a valley with optimal transport properties or two or more bands become degenerate. Alignment of additional carrier pockets translates to summation over additional sets of subband energies in Eqs. (5), (6), and (8), which could mean a substantial increase in PF for every additional band. Such "carrier pocket engineering" has been demonstrated theoretically in p-type $Bi_{1-x}Sb_x$ nanowires[32] and GaAs/AlAs superlattice structures[33] and experimentally in Si/Ge superlattice structures.[34]

(2) Decreasing the lattice thermal conductivity in nanostructures, with emphasis on a size range in which suppression of phonon heat transport more than compensates for the decrease in PF. This concept was realized in Si nanowires (∼50 nm in diameter) with roughened surfaces. The 99% decrease in total thermal conductivity more than makes up for an 18% decrease in the measured PF.[2]

(3) Altering the dominant electron scattering mechanism via nanoscale engineering of the material. A particularly successful example of this is in nanostructured bulk materials, in which either nanoinclusions are imbedded in a bulk matrix or nanoparticles are hot pressed to form bulk materials.[35–37] In both cases, the resulting grain boundaries act as low-energy electron scattering centers. Such a modification in the energy dependence of $\tau(E)$ can increase the Seebeck coefficient by increasing the asymmetry about the Fermi energy in the integrand of $\mathbf{L}^{(1)}$ in Eq. (2). Utilizing this technique, improvements in PF values over bulk have been demonstrated in $In_{0.53}Ga_{0.47}As$ with random ErAs nanoinclusions,[38] nanostructured $Bi_xSb_{2-x}Te_3$,[39,40] and hot-pressed SiGe alloys.[41]

The results of this model are in line with the conclusion reached by Mahan and Sofo: the DOS of the ideal thermoelectric material consists of a δ-function, for which the electron energy distribution is narrowest, near the Fermi energy.[42] We have identified a minimum in the relation between PF and system size, from which point PF increases as the system is made smaller or bigger. In the first case, the subbands move farther apart, and in this single-subband regime, the spread of the electron energy distribution is minimized. In the second case, the subbands move closer together, which also leads to a reduction in the variance of the energy of the electrons now populating many subbands. While the Mahan-Sofo concept was formulated for the optimization of ZT, the reduction of the PF value of many-subband nanoscale systems relative to bulk can be qualitatively understood on the basis of this concept.

In summary, we have presented room temperature PF calculations as a function of system size for cylindrical and square nanowires and thin films for a hypothetical isotropic single-carrier semiconductor. Regardless of the specific band parameters, system geometry, and dimensionality assumed, PF exhibits the same qualitative behavior as a function of system size. For small systems (smaller than the size corresponding to the minimum PF), the conduction band effectively consists of a single subband, and PF increases as the size decreases until the CRTA breaks down. For larger systems, on the other hand, the number of contributing subbands increases with system size, leading to an increase in PF.

We developed universal curves of the optimized PF as a function of system size for nanostructures (cylindrical nanowires, square nanowires, and thin films) that apply to any single-carrier isotropic semiconductor *regardless of its specific band parameters*. These universal scaling relations are important in understanding the thermoelectric behavior of nanostructured materials: given just two material parameters (carrier effective mass and mobility), the universal curves can be scaled to provide PF for any system size with minimal computational effort. In particular, the system size corresponding to the minimum PF value and the largest system size for which an improvement in PF is seen over bulk are easily determined. Universal PF curves can be constructed for other structures (e.g. of lower symmetry) following the approach described here.

ACKNOWLEDGMENT

This work was supported by the Minta Martin Foundation. J.E.C. acknowledges an Achievement Rewards for College Scientists Foundation scholarship.

---

[*] oded@umd.edu

[1] G. S. Nolas, J. Sharp, and H. J. Goldsmid, *Thermoelectrics: Basic Principles and New Materials Developments* (Springer, Berlin, 2001).

[2] A. I. Hochbaum, R. Chen, R. D. Delgado, W. Liang, E. C. Garnett, M. Najarian, A. Majumdar, and P. Yang, Nature **451**, 163 (2008).

[3] C. J. Vineis, T. C. Harman, S. D. Calawa, M. P. Walsh, R. E. Reeder, R. Singh, and A. Shakouri, Phys. Rev. B **77**, 235202 (2008).

[4] S. K. Bux, R. G. Blair, P. K. Gogna, H. Lee, G. Chen, M. S. Dresselhaus, R. B. Kaner, and J.-P. Fleurial, Adv. Funct. Mater. **19**, 2445 (2009).

[5] J. Tang, H.-T. Wang, D. H. Lee, M. Fardy, Z. Huo, T. P. Russell, and P. Yang, Nano Lett. **10**, 4279 (2010).

[6] A. I. Boukai, Y. Bunimovich, J. Tahir-Kheli, J.-K. Yu, W. A. Goddard III, and J. R. Heath, Nature **451**, 168 (2008).

[7] L. D. Hicks and M. S. Dresselhaus, Phys. Rev. B **47**, 16631 (1993).

[8] L. D. Hicks and M. S. Dresselhaus, Phys. Rev. B **47**, 12727 (1993).

[9] F. Stern and W. E. Howard, Phys. Rev. **163**, 816 (1967).

[10] J. E. Cornett and O. Rabin, Appl. Phys. Lett. **98**, 182104 (2011).

[11] N. W. Ashcroft and N. D. Mermin, *Solid State Physics* (Holt, Rinehart and Winston, New York, 1976).

[12] Y.-M. Lin, M. Sc. Thesis, Massachusetts Institute of Technology, Cambridge, Massachusetts, 2000.

[13] Y.-M. Lin, X. Sun, and M. S. Dresselhaus, Phys. Rev. B **62**, 4610 (2000).

[14] A. J. Levin, M. R. Black, and M. S. Dresselhaus, Phys. Rev. B **79**, 165117 (2009).

[15] D. A. Broido and T. L. Reinecke, Phys. Rev. B **64**, 045324 (2001).

[16] N. Mingo, Appl. Phys. Lett. **84**, 2652 (2004); see also **88**, 149902(E) (2006).

[17] N. Mingo, Appl. Phys. Lett. **85**, 5986 (2004).

[18] T. Wang, T. H. Hsieh, and T. W. Chen, J. Appl. Phys. **74**, 426 (1993).

[19] F. Gámiz, J. B. Roldán, P. Cartujo-Cassinello, J. E. Carceller, J. A. López-Villanueva, and S. Rodriguez, J. Appl. Phys. **86**, 6269 (1999).

[20] S. Jin, M. V. Fischetti, and T.-W. Tang, J. Appl. Phys. **102**, 083715 (2007).

[21] J. Hattori, S. Uno, K. Nakazato, and N. Mori, J. Appl. Phys. **107**, 033712 (2010).

[22] L. Donetti, F. Gámiz, N. Rodriguez, F. Jimenez, and C. Sampedro, Appl. Phys. Lett. **88**, 122108 (2006).

[23] D. Esseni and E. Sangiorgi, Solid State Electron. **48**, 927 (2004).

[24] M. S. P. Lucas, J. Appl. Phys. **36**, 1632 (1965).

[25] K. Fuchs, Math. Proc. Camb. Phil. Soc. **34**, 100 (1938).

[26] E. H. Sondheimer, Adv. Phys. **1**, 1 (1952).

[27] Y. Cui, Z. Zhong, D. Wang, W. U. Wang, and C. M. Lieber, Nano Lett. **3**, 149 (2003).

[28] Y. Huang, X. Duan, Y. Cui, and C. M. Lieber, Nano Lett. **2**, 101 (2002).

[29] D. A. Broido and T. L. Reinecke, in *Recent Trends in Thermoelectric Materials Research III*, edited by T. M. Tritt (Elsevier, San Diego, 2001), Vol. 71, pp. 123.

[30] D. A. Broido and T. L. Reinecke, Appl. Phys. Lett. **70**, 2834 (1997).

[31] D. A. Broido and T. L. Reinecke, Appl. Phys. Lett. **77**, 705 (2000).

[32] O. Rabin, Y.-M. Lin, and M. S. Dresselhaus, Appl. Phys. Lett. **79**, 81 (2001).

[33] T. Koga, X. Sun, S. B. Cronin, and M. S. Dresselhaus, Appl. Phys. Lett. **73**, 2950 (1998).

[34] T. Koga, S. B. Cronin, M. S. Dresselhaus, J. L. Liu, and K. L. Wang, Appl. Phys. Lett. **77**, 1490 (2000).

[35] Y. Lan, A. J. Minnich, G. Chen, and Z. Ren, Adv. Funct. Mater. **20**, 357 (2010).

[36] M. S. Dresselhaus, G. Chen, M. Y. Tang, R. G. Yang, H. Lee, D. Z. Wang, Z. F. Ren, J. P. Fleurial, and P. Gogna, Adv. Mater. **19**, 1043 (2007).

[37] C. J. Vineis, A. Shakouri, A. Majumdar, and M. G. Kanatzidis, Adv. Mater. **22**, 3970 (2010).

[38] W. Kim, J. Zide, A. Gossard, D. Klenov, S. Stemmer, A. Shakouri, and A. Majumdar, Phys. Rev. Lett. **96**, 045901 (2006).

[39] B. Poudel, Q. Hao, Y. Ma, Y. Lan, A. Minnich, B. Yu, X. Yan, D. Wang, A. Muto, D. Vashaee, X. Chen, J. Liu, M. S. Dresselhaus, G. Chen, and Z. Ren, Science **320**, 634 (2008).

[40] Y. Lan, B. Poudel, Y. Ma, D. Wang, M. S. Dresselhaus, G. Chen, and Z. Ren, Nano Lett. **9**, 1419 (2009).

[41] G. Joshi, H. Lee, Y. Lan, X. Wang, G. Zhu, D. Wang, R. W. Gould, D. C. Cuff, M. Y. Tang, M. S. Dresselhaus, G. Chen, and Z. Ren, Nano Lett. **8**, 4670 (2008).

[42] G. D. Mahan and J. O. Sofo, Proc. Nat. Acad. Sci. USA **93**, 7436 (1996).